

Thermally switchable polarization manipulation and diodelike transmission in scalable, resonator-free, mid-infrared metasurfaces with vanadium-dioxide grids

Andriy E. Serebryannikov,¹ Akhlesh Lakhtakia,² and Ekmel Ozbay³

¹*Division of Physics of Nanostructures, ISQI, Faculty of Physics, Adam Mickiewicz University, 61-614 Poznań, Poland*

²*NanoMM–Nanoengineered Metamaterials Group, Department of Engineering Science and Mechanics, Pennsylvania State University, University Park, Pennsylvania 16802, USA*

³*Nanotechnology Research Center (NANOTAM), Institute of Materials Sciences (UNAM), Department of Physics, and Department of Electrical Engineering, Bilkent University, 06800 Ankara, Turkey*
(Dated: March 25, 2022)

We conceptualized three-array scalable metasurfaces comprising only three thin strip grids and numerically demonstrated their characteristics in the mid-infrared spectral regime for switchable polarization manipulation and related asymmetric diodelike transmission (AT). A few or all of the grids were taken to be made of VO₂, a phase-change material. For each proposed metasurface, two effective structures and, therefore, two different functionalities exist, corresponding to the metallic and insulating phases of VO₂. The achieved scenarios of functionality switching that depend on the VO₂ phase are shown to significantly depend in the way in which VO₂ is incorporated to the metasurface. Switchable bands of polarization manipulation are up to 40 THz wide. The AT band can be modulated when Fabry–Perot (anti-)resonances come into play.

I. INTRODUCTION

Polarization manipulation and related asymmetric transmission (AT) achievable *via* quasipolar metasurfaces constitute a topic of considerable attention from the mid-2000's. Most researchers were initially focused on few-layer metasurfaces comprising coupled periodic arrays of (complementary) subwavelength resonators [1–6]. Later, geometric-phase gradient metasurfaces were proposed for polarization control [7, 8]. Recently, metasurfaces and heterostructures enabling efficient manipulation by orbital angular momentum have been suggested [9]. Notably, a single-array structure can deliver polarization manipulation/conversion with AT for incident circularly polarized (CP) plane waves, but at least two coupled arrays are needed for AT when the incident plane wave is linearly polarized (LP). Mid-infrared (MIR) and near-infrared applications need rather simple design solutions to assure facile fabrication. In particular, polarization-converting, few-layer, resonator-free anisotropic structures comprising grids and related components have been suggested for different parts of electromagnetic spectrum [10–12]. Such structures are often considered to be dispersionless and, therefore, promising for applications.

The research landscape for polarization control changed dramatically when tunable materials were introduced to metasurfaces and metamaterials, thereby enabling reconfigurable and multifunctional devices [13–15]. Magnetically, electrically, thermally, and optically tunable materials such as graphene, InAs, InSb, GeTe, CdTe, VO₂, and ITO are often considered, in this context. In particular, VO₂ is a thermally tunable phase-change material useful from the terahertz (THz) to the visible spectral regimes [16–19]. Transition from an insulator (I) phase to a metallic (M) phase, or from M to I

phase, under the variation of a control parameter may occur for many natural materials [20]. One of them is vanadium dioxide (VO₂), an attractive phase-change material displaying a hysteretic insulator-metal-insulator transition [21]. It is underlain by the monoclinic-to-tetragonal phase change that occurs as temperature, T is raised from a value slightly lower than 58 °C to a value slightly above 72 °C [22]. As a result, VO₂ behaves as a dissipative insulator (i-VO₂) when monoclinic and metallic (m-VO₂) when tetragonal, provided the free-space wavelength $\lambda \gtrsim 1300$ nm.

The simplest form in which VO₂ has been used in photonic heterostructures and metasurfaces is thin homogeneous layers [23–25], but the variety of functionality-switching scenarios then is limited. VO₂ pads/inserts have been incorporated in metallic subwavelength resonators for THz applications, especially for switchable polarization manipulation and AT [26–29]. However, the feasibility of such meta-atoms is questionable for MIR applications. Meta-atoms comprising only VO₂ or another thermally tunable material have also been proposed, to exploit resonances in m-VO₂ and/or i-VO₂ [30–37]. Patterned thin films of a phase-change material have been utilized either to directly enable tunability or indirectly tune a functionality enabled by other components [38–42].

In this paper, we conceptualize and numerically justify the potential of three-array metasurfaces comprising only VO₂ grids and Ag grids, which are capable of thermally switchable wideband polarization manipulation and diodelike AT for LP waves in the MIR regime. The motivation for this study includes avoidance of subwavelength resonators (made of either a metal or a phase change material, or both) to prevent possible resonance enhancement of absorption. The particular aims are to: (a) demonstrate the role of VO₂ phase change as enabler of the functionality-switching scenarios involving polar-

ization conversion and AT; (b) clarify the way of using how VO₂ in the grids affects the particular switching scenarios; (c) demonstrate scalability of the proposed designs in the MIR regime for wider applicability; (d) show that conduction and dissipation in m-VO₂ are suitable to replace a metal so that the capability for polarization manipulation remains high; and (e) clarify the emergence and role of Fabry-Perot resonances in the resulting functionality and scalability. Geometrically, the studied structures remind ones proposed by others in [10, 12], in contrast to which a phase-change material is used by us both as a functionality enabling material and as a material for tunable components. Taking into account that the required thickness of VO₂ strips ranges only from 40 to 180 nm, and that m-VO₂ is not such a good conductor as Cu or Ag, the capability of the structures comprising VO₂ grids for polarization manipulation is not evident and needs justification. The studied metasurfaces are easy to fabricate by using the standard techniques. Maximization of AT contrast and on-off switching contrast are beyond the scope.

II. RESULTS AND DISCUSSION

Metasurfaces of three types are considered, differing in the way in which VO₂ is used. Every metasurface was assumed to be illuminated by a normally incident LP plane wave. CST Studio Suite [43] was used to calculate the transmission coefficients τ_{nm}^M and τ_{nm}^I , where the subscripts $m \in \{x, y\}$ and $n \in \{x, y\}$, respectively, identify the direction of the electric field of the incident LP plane wave and the direction of the transmitted electric field in the far zone. Front-face and back-face illuminations correspond to the propagation along the $-z$ and $+z$ directions, respectively. These cases are identified by the superscripts \rightarrow and \leftarrow . The considered structure is Lorentz reciprocal [44], so $|\tau_{xy}^{\rightarrow}| = |\tau_{yx}^{\leftarrow}|$, $|\tau_{xx}^{\rightarrow}| = |\tau_{xx}^{\leftarrow}|$, $|\tau_{xy}^{\leftarrow}| = |\tau_{yx}^{\rightarrow}|$, and $|\tau_{yx}^{\rightarrow}| = |\tau_{xy}^{\leftarrow}|$. Asymmetry in transmission may be desirably strong when either (a) $|\tau_{xy}^{\rightarrow}| \gg |\tau_{xy}^{\leftarrow}|$ and $|\tau_{xy}^{\rightarrow}| \gg |\tau_{xx}^{\rightarrow}|$, or (b) $|\tau_{xy}^{\rightarrow}| \ll |\tau_{xy}^{\leftarrow}|$ and $|\tau_{xx}^{\rightarrow}| \ll |\tau_{xy}^{\leftarrow}|$. The complex relative permittivity of VO₂ was calculated from available experimental data [45]. The Drude model of the complex relative permittivity of Ag was used, i.e., $\varepsilon_r^{Ag}(\omega) = 1 - (\omega_p^{Ag})^2 / [\omega(\omega + i\gamma)]$, where $\omega = 2\pi f$ is the angular frequency and f is the linear frequency, the angular plasma frequency $\omega_p^{Ag} = 1.37 \times 10^{16}$ rad s⁻¹, and the collision frequency is $\gamma = 2.73 \times 10^{13}$ rad s⁻¹ [46].

A. Case of the central grid made of VO₂

First, we consider the metasurfaces 1A–1F, each with a VO₂ grid separated from two Ag grids by dielectric spacers with the central grid oriented at 45° in the transverse plane with respect to the other two grids, as shown in Fig. 1(a). Thus, each metasurface has two conducting grids for i-VO₂ and three conducting grids for m-

VO₂. The central grid works like a phase screen for i-VO₂, as we have recently shown [42]. Accordingly, switching is possible between transmission with the dominant cross-polarized components for m-VO₂ and reflection for i-VO₂. Graphs of the transmission-coefficient magnitudes vs. f are presented for all six metasurfaces in Figs. 1(b)–(g). Let $\psi = |\tau_{yx}^{M\rightarrow}|^2 / |\tau_{xx}^{M\rightarrow}|^2$ and $\zeta = (|\tau_{yx}^{M\rightarrow}|^2 + |\tau_{xx}^{M\rightarrow}|^2) / (|\tau_{yx}^{I\rightarrow}|^2 + |\tau_{xx}^{I\rightarrow}|^2)$. Switchable AT appears, for instance, at $f = 64$ THz in Fig. 1(b) for metasurface 1A, where $\psi = 87$ and $\zeta = 8.2$, and at $f = 37$ THz in Fig. 1(e) for metasurface 1D, where $\psi = 147$ and $\zeta = 10$. Similar transmission features are observed in Figs. 1(b)–(d) for metasurfaces 1A–1C as in Figs. 1(e)–(g) for metasurfaces 1D–1F, the spacers in the first three metasurfaces being two-thirds in thickness compared to those in the last three metasurfaces.

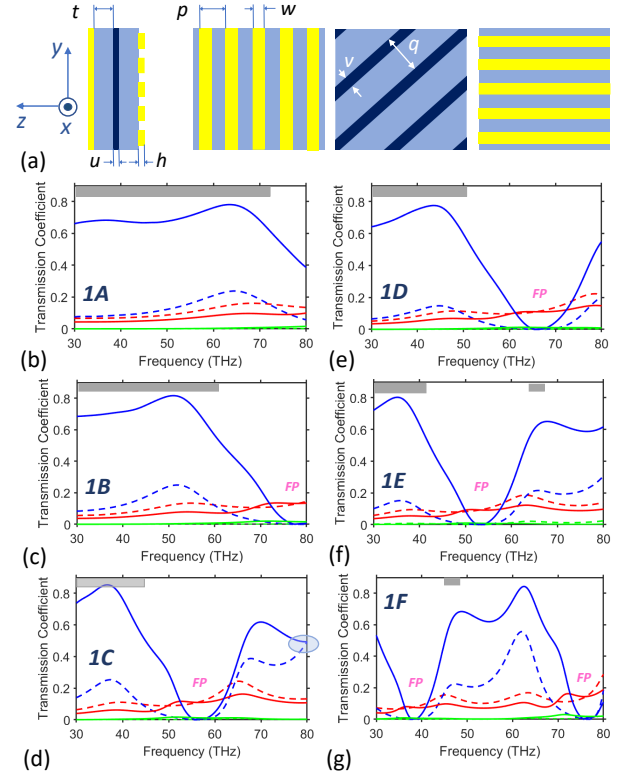


FIG. 1. Spectrums of transmission-coefficient magnitudes for six metasurfaces, 1A to 1F, each comprising a VO₂ grid (shown in dark blue) separated from two Ag grids (yellow) by dielectric spacers (light blue). The central grid is oriented at 45° with respect to the other two grids in the xy plane. (a) From left to right: side cross-section view, front view, mid cross-section view, and back view. (b)–(g) Transmission spectrums for spacer thickness (b, c, d) $t = 1000$ nm and (e, f, g) $t = 1500$ nm, when relative permittivity of spacer $\varepsilon_{sp} = 2.1$, $h = 50$ nm, $p = 600$ nm, $w = p/2$, $q = \sqrt{2}p$, $u = 2h$, and $v = w$; scaling coefficient (b,e) $s = 1$, (c,f) 1.25, and (d,g) 1.75. Solid lines: m-VO₂, dashed lines: i-VO₂; blue lines: $|\tau_{yx}^{\rightarrow}|$, green lines: $|\tau_{xy}^{\rightarrow}|$, and red lines: $|\tau_{xx}^{\rightarrow}| = |\tau_{yy}^{\rightarrow}|$. Grey rectangles indicate the f -ranges which may be suitable for switchable AT.

As metasurfaces 1A and 1D differ only in spacer thickness t , their transmission features are *mutually scalable*, albeit approximately; the same statement can be made about metasurfaces 1B and 1E, as well as about metasurfaces 1C and 1F. This scaling can be approximately quantified by comparing the spectral locations of the typical minimums and maximums. Spectral features are downshifted and compressed in the f -domain when the scaling coefficient s is increased. For instance, the minimum of $|\tau_{yx}^{M\rightarrow}|$ occurs at 65 THz for 1D [Fig. 1(e)], 53 THz for 1E [Fig. 1(f)], and 38 THz for 1F [Fig. 1(g)], in inverse proportion to the spacer thickness. In contrast with conventional Fabry–Perot anti-resonances which appear for a homogeneous dielectric slab, all minimums of $|\tau_{yx}^{M\rightarrow}|$ in Figs. 1(b)–(g) correspond to the condition $2\varepsilon_{sp}^{1/2}kt \approx \ell\pi$, where ε_{sp} is the relative permittivity of the spacer, $k = 2\pi/\lambda$ is the free-space wavenumber, and $\ell \in \{1, 2\}$. These minimums, identified by *FP* in the graphs, have the same spectral locations as the maximums in the case of a homogeneous slab dielectric slab sandwiched by the two parallel Ag grids, i.e., when the back-face grid is not rotated with respect to front-face grid. Notably, most of the energy of the incident plane wave is reflected at the minimums of $|\tau_{yx}^{M\rightarrow}|$, while reflections are weak at the maximums of $|\tau_{yx}^{M\rightarrow}|$. By adjusting the spacer thickness, we can obtain on-off switchable, diodelike AT with a desired bandwidth.

Incidentally, $|\tau_{yx}^{\rightarrow}|$ can be insensitive to the phase of VO₂ at a particular frequency, e.g., $|\tau_{yx}^{I\rightarrow}| = |\tau_{yx}^{M\rightarrow}|$ at 80 THz in Fig. 1(d) for 1C (shown by a bluish ellipse). On the other hand, different maximums of $|\tau_{yx}^{M\rightarrow}|$ show different sensitivity to the crystallographic phase of VO₂. For instance, in Fig. 1(g) for 1F, $\zeta \approx 10$ at 47 THz but $\zeta \approx 2$ at 62 THz.

B. Case of the outer grids made of VO₂

Next, let us swap Ag and VO₂ in metasurfaces 1A–1F to form metasurfaces 2A–2F, each with an Ag grid separated from two VO₂ grids by dielectric spacers, as shown in Fig. 2(a). In this case, each metasurface has one conducting grid for i-VO₂ and three conducting grids for m-VO₂. The front-face and the back-face grids work like a phase screen for i-VO₂ [42]. For m-VO₂, the cross-polarized component of the transmitted plane wave is dominant compared to the co-polarized one, i.e., $\psi > 10$. In particular, $\psi = 11.7$ at 50 THz in Fig. 2(b) for 2A, 19.7 at 30 THz in Fig. 2(c) for 2B, and 28.4 at 62 THz in Fig. 2(g) for 2F. For i-VO₂, none of the transmission components is suppressed, i.e., they all are of the same order of magnitude. Thus, transmission mode is conserved when the crystallographic phase of VO₂ is thermally altered in 2A–2F, this characteristic being absent in Fig. 1 for 1A–1F. Moreover, spectral regimes with $|\tau_{yx}^{I\rightarrow}| \approx |\tau_{xx}^{I\rightarrow}| \approx |\tau_{xy}^{I\rightarrow}| \approx |\tau_{yy}^{I\rightarrow}|$ are observed (shown by yellowish circles). Then, both co- and cross-polarized

transmission channels contain *equal energy*, regardless of whether the front face or the back face is illuminated. It is evident at $f = 80$ THz in Fig. 2(c) for 2B and at $f = 55$ THz in Fig. 2(f) for 2E.

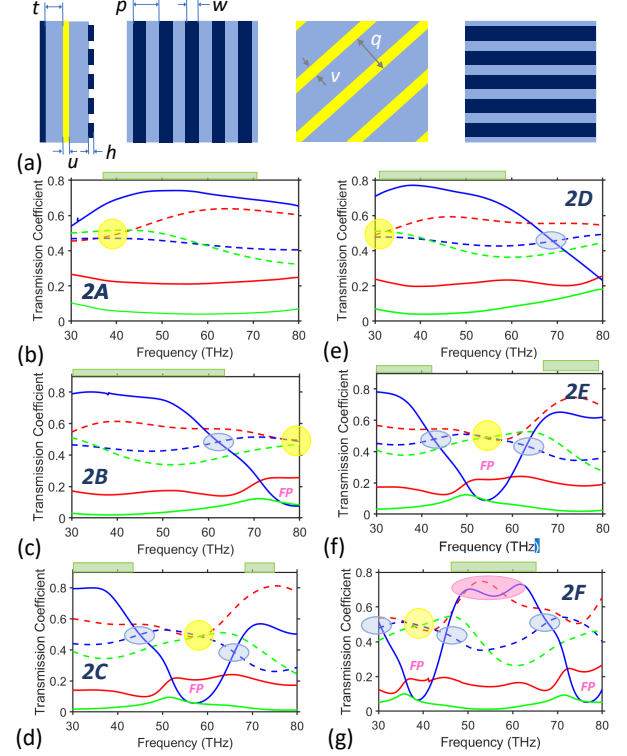


FIG. 2. Same as Fig. 1 but for metasurfaces 2A–2F, each comprising an Ag grid (shown in yellow) separated from VO₂ grids (dark blue) by dielectric spacers (light blue). Scaling coefficient (b,e) $s = 0.75$, (c,f) 1.25, and (d,g) 1.75. Light green rectangles in each plot indicate the f -ranges which may be suitable for AT when m-VO₂ is used.

The features observed in Figs. 2(e)–(g) are similar to the ones in Figs. 2(b)–(d), so that a desired modulation of the transmission spectrum can be adjusted via variations in t by means of Fabry–Perot resonances and anti-resonances, as well as a desired location of the AT band for m-VO₂ and the equal-energy regime for i-VO₂. These bands may coincide or not coincide, depending on which functionality-switching scenario is needed. Scaling manifests itself in Fig. 2, similarly to Fig. 1, in the redshift of transmission features with increase of the scaling coefficient s . In addition, transmission spectrum becomes more compressed when a thicker spacer is used. Despite the structures and functional capabilities of the metasurfaces 2A–2F being different from those of the metasurfaces 1A–1F, the insensitivity of the latter to the crystallographic phase of VO₂ is also exhibited by the former for specific spectral regimes and field components (bluish ellipses). This is exemplified by $|\tau_{yx}^{\rightarrow}|$, e.g., at $f = 62$ THz in Fig. 2(c) for 2B and 43 THz as well as 63 THz in Fig. 2(f) for 2E. The number of the related spectral

regimes, in which the insensitivity is observed within the considered f -range, increases with t , since the transmission spectrum thereby becomes more compressed as the spacer thickens.

Among the switching regimes achievable with 2A–2F, the one observed in Fig. 2(g) for $f \in [45, 60]$ THz should be mentioned. Here, the strongest transmission component has nearly the same magnitude, but represents either the co- or the cross-polarized component for the same incident plane wave, depending on which crystallographic phase of VO₂ is used (rosy ellipse).

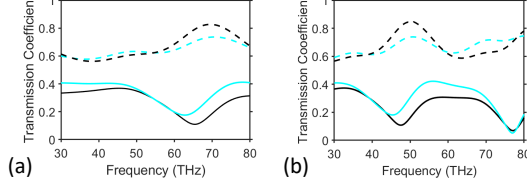


FIG. 3. Linear-to-circular polarization conversion for metasurfaces (a) 2C and (b) 2F. Dashed cyan lines: $|\tau_{Rx}|$, solid cyan lines: $|\tau_{Lx}|$, dashed black lines: $|\tau_{Ry}|$, and solid black lines: $|\tau_{Ly}|$.

For i-VO₂, the metasurfaces 2A–2F can efficiently transmit an incident LP wave as a plane wave whose polarization state is close to being circular. We have adopted the usual optics convention: an LCP (left-handed CP) wave satisfies the condition $\nabla \times \vec{E} = k\vec{E}$, whereas an RCP (right-handed CP) wave satisfies the condition $\nabla \times \vec{E} = -k\vec{E}$. Figure 3 presents transmission results for metasurfaces 2C and 2F, but the transmission is quantified now for CP outgoing waves. As observed in Fig. 3, both $|\tau_{Rx}|/|\tau_{Lx}| > 1$ and $|\tau_{Ry}|/|\tau_{Ly}| > 1$ for both selected metasurfaces. Moreover, spectral regimes exist in which $|\tau_{Rx}|/|\tau_{Lx}| > 5$ and/or $|\tau_{Ry}|/|\tau_{Ly}| > 5$, so that linear-to-(nearly-)circular polarization conversion (LCPC) takes place. The selective coupling of the incident LP waves to the outgoing CP waves allows the AT ranges for m-VO₂ and LCPC ranges for m-VO₂ to overlap when s and t are properly adjusted. In this case, change of phase of VO₂ results in bifunctional operation at fixed f . Otherwise, bifunctionality is obtained while using different f -ranges for the two phases of VO₂.

C. Case of a metal-free structure

Finally, we consider the case of metal-free metasurfaces, i.e., when all three grids are made of VO₂. As a result, every metasurface in Fig. 4 has three conducting grids for m-VO₂ but comprises only insulators for i-VO₂. Accordingly, we obtain AT for m-VO₂ and predominantly co-polarized, weakly attenuated transmission for i-VO₂. This scenario of functionality switching is totally new as compared to the ones in Figs. 1 and 2, and this is the main reason why we want to abandon metals.

The results are presented in Figs. 4(b)–(e) for the same geometric parameters as for Figs. 1(b), (c), (d), and (g).

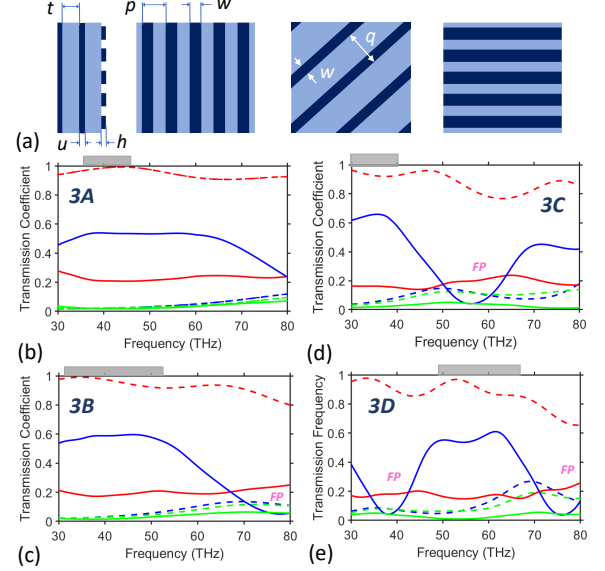


FIG. 4. Spectrums of transmission-coefficient magnitudes calculated for four metasurfaces, labeled 3A to 3D, each comprising three VO₂ grids (shown in dark blue) separated by dielectric spacers (light blue). (a) From left to right: side cross-section view, front view, mid cross-section view, and back view, respectively. (b)–(e) Transmission spectrums for spacer thickness (b, c, d) $t = 1000$ nm and (e) $t = 1500$ nm. Scaling coefficient (b) $s = 0.75$, (c) 1.25 and (d,e) 1.75. See Fig. 1 for other details.

The value of ψ in Fig. 4 typically does not exceed 10. For instance, $\psi = 6.5$ at 38 THz in Fig. 4(b) for 3A, $\psi = 7$ at 38 THz in Fig. 4(c) for 3B, and $\psi = 12$ at 62 THz in Fig. 4(e) for 3D. Along with the achievable magnitude of $|\tau_{yx}^{M \rightarrow}|$, this result is quite good since the metasurfaces do not contain any metal or cylindrical or other volume dielectric resonators (in contrast, say, with Ref. 34). Also for these metasurfaces we obtain scaling as the redshift of the basic transmission features occurring with increase of s , as observed from a comparison of Figs. 4(b), 4(c) and 4(d), in spite of VO₂ being dispersive. Notably, the shifts of the minimums of $|\tau_{yx}^{M \rightarrow}|$ and the edges of the strong transmission ranges occur due to change of either s or t , so these parameters provide two degrees of freedom for designing the transmission spectrum.

III. CONCLUSION

To summarize, we studied transmission through few-array metasurfaces comprising only three strip grids and exhibiting switchable polarization manipulation and related AT for LP plane waves in the 30–80-THz frequency

range. The proposed structures are approximately scalable within this spectral regime. Subwavelength resonators, inserts, and pads are not needed that is important for ease of fabrication at MIR frequencies. Diverse scenarios of functionality switching can be achieved, depending on whether VO₂ is used as the material of only the two outer, only the central, or all three grids. In all scenarios, well-pronounced AT connected with polarization manipulation occurs for m-VO₂. It is switched for another functionality when m-VO₂ is changed to i-VO₂. This is true also when all three grids are made of VO₂, i.e., the metasurface is metal-free. Fabry–Perot (anti-)resonances manifest themselves in a way different from the case of a homogeneous dielectric slab of the same of thickness as two spacers in the studied structures and enable efficient modulation of the polarization effects and transmission. The observed capability for po-

larization manipulation and AT remains while adding a semi-infinite dielectric substrate at the back side (results are not shown). Besides the studied metasurfaces, those with only the front-face grid made of VO₂ were examined (results are not shown). The transmission efficiency can further be increased by using wider strips of the central grid than in the presented examples. For instance, $|\tau_{yx}^{M \rightarrow}| \approx 0.8$ and 0.7 were obtained in the AT bands for the metasurfaces similar to 1F and 3D, respectively.

ACKNOWLEDGMENTS

This work was supported by Narodowe Centrum Nauki, Project UMO-2020/39/I/ST3/02413. A. L. thanks the Charles Godfrey Binder Endowment at the Pennsylvania State University for ongoing support. E. O. thanks the Turkish Academy of Sciences for partial support.

-
- [1] C. Menzel, C. Helgert, C. Rockstuhl, E.-B. Kley, A. Tünnermann, T. Pertsch, and F. Lederer, Asymmetric transmission of linearly polarized light at optical metamaterials, *Phys. Rev. Lett.* **104**, 253902 (2010).
 - [2] V. Fedotov, P. Mladonov, S. Prosvirnin, A. Rogacheva, Y. Chen, and N. Zheludev, Asymmetric propagation of electromagnetic waves through a planar chiral structure, *Phys. Rev. Lett.* **97**, 167401 (2006).
 - [3] M. Mutlu, S. Cakmakyapan, A. E. Serebryannikov, and E. Ozbay, One-way reciprocal spoof surface plasmons and relevant reversible diodelike beaming, *Phys. Rev. B* **87**, 205123 (2013).
 - [4] C. Huang, Y. Feng, J. Zhao, Z. Wang, and T. Jiang, Asymmetric electromagnetic wave transmission of linear polarization via polarization conversion through chiral metamaterial structures, *Phys. Rev. B* **85**, 195131 (2012).
 - [5] S. Yan and G. A. Vandenbosch, Compact circular polarizer based on chiral twisted double split-ring resonator, *Appl. Phys. Lett.* **102**, 103503 (2013).
 - [6] A. E. Serebryannikov, M. Mutlu, and E. Ozbay, Dielectric inspired scaling of polarization conversion subwavelength resonances in open ultrathin chiral structures, *Appl. Phys. Lett.* **107**, 221907 (2015).
 - [7] J. B. Mueller, N. A. Rubin, R. C. Devlin, B. Groever, and F. Capasso, Metasurface polarization optics: independent phase control of arbitrary orthogonal states of polarization, *Phys. Rev. Lett.* **118**, 113901 (2017).
 - [8] W. Luo, S. Sun, H.-X. Xu, Q. He, and L. Zhou, Transmissive ultrathin pancharatnam–berry metasurfaces with nearly 100% efficiency, *Phys. Rev. Appl.* **7**, 044033 (2017).
 - [9] K. Zhang, Y. Yuan, X. Ding, H. Li, B. Ratni, Q. Wu, J. Liu, S. N. Burokur, and J. Tan, Polarization-engineered noninterleaved metasurface for integer and fractional orbital angular momentum multiplexing, *Laser Photon. Rev.* **15**, 2000351 (2021).
 - [10] C. Pfeiffer, C. Zhang, V. Ray, L. J. Guo, and A. Grbic, High performance bianisotropic metasurfaces: asymmetric transmission of light, *Phys. Rev. Lett.* **113**, 023902 (2014).
 - [11] Y. Zhao, M. Belkin, and A. Alù, Twisted optical metamaterials for planarized ultrathin broadband circular polarizers, *Nat. Commun.* **3**, 870 (2012).
 - [12] C. Zhang, C. Pfeiffer, T. Jang, V. Ray, M. Junda, P. Uprety, N. Podraza, A. Grbic, and L. J. Guo, Breaking Malus’ law: highly efficient, broadband, and angular robust asymmetric light transmitting metasurface, *Laser Photon. Rev.* **10**, 791 (2016).
 - [13] Q. Wang, E. T. Rogers, B. Gholipour, C.-M. Wang, G. Yuan, J. Teng, and N. I. Zheludev, Optically reconfigurable metasurfaces and photonic devices based on phase change materials, *Nat. Photon.* **10**, 60 (2016).
 - [14] E. Maguid, I. Yulevich, M. Yannai, V. Kleiner, M. L. Brongersma, and E. Hasman, Multifunctional interleaved geometric-phase dielectric metasurfaces, *Light Sci. Appl.* **6**, e17027 (2017).
 - [15] P. Kumar, A. Lakhtakia, and P. K. Jain, Tricontrollable pixelated metasurface for stopband for terahertz radiation, *J. Electromag. Waves Appl.* **34**, 2065 (2020).
 - [16] S. Cueff, J. John, Z. Zhang, J. Parra, J. Sun, R. Orobtcouk, S. Ramanathan, and P. Sanchis, VO₂ nanophotonics, *APL Photon.* **5**, 110901 (2020).
 - [17] K. Liu, S. Lee, S. Yang, O. Delaire, and J. Wu, Recent progresses on physics and applications of vanadium dioxide, *Mater. Today* **21**, 875 (2018).
 - [18] H. Lu, S. Clark, Y. Guo, and J. Robertson, The metal–insulator phase change in vanadium dioxide and its applications, *J. Appl. Phys.* **129**, 240902 (2021).
 - [19] R. Shi, N. Shen, J. Wang, W. Wang, A. Amini, N. Wang, and C. Cheng, Recent advances in fabrication strategies, phase transition modulation, and advanced applications of vanadium dioxide, *Appl. Phys. Rev.* **6**, 011312 (2019).
 - [20] M. Imada, A. Fujimori, and Y. Tokura, Metal–insulator transitions, *Rev. Mod. Phys.* **70**, 1039 (1998).
 - [21] D. Adler, Mechanisms for metal–nonmetal transitions in transition-metal oxides and sulfides, *Rev. Mod. Phys.* **40**, 714 (1968).
 - [22] H. Kakiuchida, P. Jin, S. Nakao, and M. Tazawa, Optical properties of vanadium dioxide film during semiconductive–metallic phase transition, *Jap. J. Appl.*

- Phys. **46**, L113 (2007).
- [23] R. Singh, A. K. Azad, Q. Jia, A. J. Taylor, and H.-T. Chen, Thermal tunability in terahertz metamaterials fabricated on strontium titanate single-crystal substrates, *Opt. Lett.* **36**, 1230 (2011).
 - [24] M. A. Kats, D. Sharma, J. Lin, P. Genevet, R. Blanchard, Z. Yang, M. M. Qazilbash, D. Basov, S. Ramanathan, and F. Capasso, Ultra-thin perfect absorber employing a tunable phase change material, *Appl. Phys. Lett.* **101**, 221101 (2012).
 - [25] M. Seo, J. Kyoung, H. Park, S. Koo, H.-s. Kim, H. Bernien, B. J. Kim, J. H. Choe, Y. H. Ahn, H.-T. Kim, *et al.*, Active terahertz nanoantennas based on VO₂ phase transition, *Nano Lett.* **10**, 2064 (2010).
 - [26] T. Lv, Y. Li, H. Ma, Z. Zhu, Z. Li, C. Guan, J. Shi, H. Zhang, and T. Cui, Hybrid metamaterial switching for manipulating chirality based on VO₂ phase transition, *Sci. Rep.* **6**, 23186 (2016).
 - [27] C. Zhang, G. Zhou, J. Wu, Y. Tang, Q. Wen, S. Li, J. Han, B. Jin, J. Chen, and P. Wu, Active control of terahertz waves using vanadium-dioxide-embedded metamaterials, *Phys. Rev. Appl.* **11**, 054016 (2019).
 - [28] X. Liu, Q. Wang, X. Zhang, H. Li, Q. Xu, Y. Xu, X. Chen, S. Li, M. Liu, Z. Tian, *et al.*, Thermally dependent dynamic meta-holography using a vanadium dioxide integrated metasurface, *Adv. Opt. Mater.* **7**, 1900175 (2019).
 - [29] M. Liu, Q. Xu, X. Chen, E. Plum, H. Li, X. Zhang, C. Zhang, C. Zou, J. Han, and W. Zhang, Temperature-controlled asymmetric transmission of electromagnetic waves, *Sci. Rep.* **9**, 4097 (2019).
 - [30] N. A. Butakov, I. Valmianski, T. Lewi, C. Urban, Z. Ren, A. A. Mikhailovsky, S. D. Wilson, I. K. Schuller, and J. A. Schuller, Switchable plasmonic-dielectric resonators with metal-insulator transitions, *ACS Photon.* **5**, 371 (2018).
 - [31] T. Paik, S.-H. Hong, E. A. Gaulding, H. Caglayan, T. R. Gordon, N. Engheta, C. R. Kagan, and C. B. Murray, Solution-processed phase-change VO₂ metamaterials from colloidal vanadium oxide (VO_x) nanocrystals, *ACS Nano* **8**, 797 (2014).
 - [32] A. E. Serebryannikov, K. B. Alici, E. Ozbay, and A. Lakhtakia, Thermally sensitive scattering of terahertz waves by coated cylinders for tunable invisibility and masking, *Opt. Express* **26**, 1 (2018).
 - [33] A. E. Serebryannikov, A. Lakhtakia, M. Aalizadeh, E. Ozbay, and G. A. Vandenbosch, Temperature-mediated invocation of the vacuum state for switchable ultrawide-angle and broadband deflection, *Sci. Rep.* **8**, 15044 (2018).
 - [34] P. Kopic, F. Ligmajer, M. Hrton, H. Ren, L. d. S. Menezes, S. A. Maier, and T. Sikola, Optically tunable mie resonance VO₂ nanoantennas for metasurfaces in the visible, *ACS Photon.* **8**, 1048 (2021).
 - [35] A. Tripathi, J. John, S. Kruk, Z. Zhang, H. S. Nguyen, L. Berguiga, P. R. Romeo, R. Orobtcouk, S. Ramanathan, Y. Kivshar, *et al.*, Tunable mie-resonant dielectric metasurfaces based on VO₂ phase-transition materials, *ACS Photon.* **8**, 1206 (2021).
 - [36] A. E. Serebryannikov, A. Lakhtakia, and E. Ozbay, Characteristic attributes of multiple cascaded terahertz metasurfaces with magnetically tunable subwavelength resonators, *Ann. Phys. (Berlin)* **530**, 1700252 (2018).
 - [37] Q. Xing, C. Wang, S. Huang, T. Liu, Y. Xie, C. Song, F. Wang, X. Li, L. Zhou, and H. Yan, Tunable graphene split-ring resonators, *Phys. Rev. Appl.* **13**, 041006 (2020).
 - [38] W. Lai, R. Shi, H. Yuan, G. Liu, A. Amini, and C. Cheng, Fully optically tunable and flexible composite films for enhanced terahertz control and multifunctional terahertz devices, *ACS Appl. Electron. Mater.* **3**, 3044 (2021).
 - [39] K. Dong, S. Hong, Y. Deng, H. Ma, J. Li, X. Wang, J. Yeo, L. Wang, S. Lou, K. B. Tom, *et al.*, A lithography-free and field-programmable photonic metacanvas, *Adv. Mater.* **30**, 1703878 (2018).
 - [40] H. Hajian, A. Ghobadi, A. E. Serebryannikov, B. Butun, G. A. Vandenbosch, and E. Ozbay, VO₂-hBN-graphene-based bi-functional metamaterial for mid-infrared bi-tunable asymmetric transmission and nearly perfect resonant absorption, *J. Opt. Soc. Am. B* **36**, 1607 (2019).
 - [41] T. Wang, J. He, J. Guo, X. Wang, S. Feng, F. Kuhl, M. Becker, A. Polity, P. J. Klar, and Y. Zhang, Thermally switchable terahertz wavefront metasurface modulators based on the insulator-to-metal transition of vanadium dioxide, *Opt. Express* **27**, 20347 (2019).
 - [42] A. E. Serebryannikov, A. Lakhtakia, G. A. Vandenbosch, and E. Ozbay, Transmissive terahertz metasurfaces with vanadium dioxide split-rings and grids for switchable asymmetric polarization manipulation, *Sci. Rep.* **12**, 3518 (2022).
 - [43] www.3ds.com/products-services/simulia/products/cst-studio-suite/solvers/, .
 - [44] T. G. Mackay and A. Lakhtakia, *Electromagnetic anisotropy and bianisotropy: a field guide* (World Scientific, 2019).
 - [45] M. J. Dicken, K. Aydin, I. M. Pryce, L. A. Sweatlock, E. M. Boyd, S. Walavalkar, J. Ma, and H. A. Atwater, Frequency tunable near-infrared metamaterials based on VO₂ phase transition, *Opt. Express* **17**, 18330 (2009).
 - [46] M. A. Ordal, R. J. Bell, R. W. Alexander, L. L. Long, and M. R. Querry, Optical properties of fourteen metals in the infrared and far infrared: Al, Co, Cu, Au, Fe, Pb, Mo, Ni, Pd, Pt, Ag, Ti, V, and W, *Appl. Opt.* **24**, 4493 (1985).